

A microfluidic pumping mechanism driven by non-equilibrium osmotic effects

Paul J. Atzberger^a, Samuel Isaacson^b, Charles S. Peskin^c

^a Department of Mathematics and Mechanical Engineering, University of California Santa Barbara, 6712 South Hall, 93106 Santa Barbara, CA, United States

^b Department of Mathematics, University of Utah, 155 South 1400 East, Room 233, Salt Lake City, UT 84112, United States

^c Courant Institute of Mathematical Sciences, New York University, New York, NY 10012, United States

article info

Article history:

Received 27 May 2008

Received in revised form

9 November 2008

Accepted 30 March 2009

Available online 14 April 2009

Communicated by D. Lohse

Keywords:

Microfluidics

Fluid dynamics

Osmosis

Reaction–diffusion–advection system

Immersed boundary method

Finite volume method

abstract

A mechanism is presented which drives a fluid flow using two chemically reacting molecular species and osmotic effects. For concreteness the mechanism is discussed in the context of a tube which at each end has a capping membrane which is permeable to the fluid but impermeable to the two molecular species. The chemical reactions occur at sites embedded in the capping membrane. Labeling the two chemical species *A* and *B*, at one end the reactions split each molecule of species *B* into two molecules of species *A*. On the other end two molecules of species *A* are fused together to form a single molecule of species *B*. A mathematical model of the solute diffusion, fluid flow, and osmotic effects is presented and used to describe the non-equilibrium steady-state flow rate generated. Theoretical and computational results are given for how the flow rate depends on the relative diffusivities of the solute species and the geometry of the system. An interesting feature of the pump is that for the same fixed chemical reactions at the tube ends, fluid flows can be driven in either direction through the tube, with the direction depending on the relative diffusivities of the solute species. The theoretical results are compared with three-dimensional numerical simulations of the pump.

© 2009 Elsevier B.V. All rights reserved.

1. Introduction

In recently proposed technological devices and in many biological systems, gradients in fluid pressure are generated by osmotic effects to drive a flow [2–9]. Osmosis occurs when solute molecules immersed in a fluid are confined within a region delineated by a boundary less permeable to molecules of the solute than the fluid. When the boundary in question is rigid, this results in a pressure exerted on the confining boundary, which exceeds that of the solvent pressure, with a dependence on the concentration of the solute and the temperature of the system. This additional pressure in the system is referred to as the “osmotic pressure”. For systems in which the confining boundary is flexible, swelling can also occur as water flows into the confining region, increasing its volume until the elastic stresses in the flexible walls have built up enough to balance the osmotic pressure [10,8], which meanwhile has been somewhat reduced by the dilution of the confined solute.

Various microfluidic pumps and actuator devices have been proposed which exploit osmosis either making use of swelling structures or electrostatic effects [1,6,7,11]. In [6,7,11] osmotic swelling is exploited to generate forces in a microactuator or to

generate deformations in vessels containing a drug for delivery. In [8,9] propulsion mechanisms are proposed which make use of a concentration gradient in the environment which induces unbalanced osmotic pressures on a small particle or lipid vesicle. In [1] an electrostatic field drives a fluid flow through a flux of ions which develops in a boundary layer of the charged wall of the pump.

In cell biology, osmotic effects play an important role. Within cells and organelles there are high concentrations of charged proteins and counter-ions. The effects of osmotic pressure must be actively mitigated by ion pumps or other means to avoid excessive swelling which could burst the cell or organelle [12,13]. Regulation of the volume of such structures can be used to drive an in-flux or out-flux of fluid which may be important in many biological processes in the cell [14,3]. Osmotic effects are also thought to play an important role in tissues of epithelial cells in the kidney, liver, and intestine in which a large volume of fluid is processed each day. A number of pumping mechanisms have been proposed that make direct use of osmotic effects [15,3,16,12,17,4,18,5].

In the systems mentioned above an osmotic pressure gradient is set up either by active pumping of solute molecules from a large external store into a confined region or by an external electrostatic field. In the present work a pumping mechanism is discussed which does not require an external store of solute molecules or electrostatic effects. In the mechanism proposed here the solute molecules are recycled in the process that sets up the osmotic pressure gradient.

Corresponding author. Tel.: +1 805 679 3239.

E-mail address: atzberg@math.ucsb.edu (P.J. Atzberger).

A variety of approaches have been taken to model osmotic phenomena ranging from thermodynamic relations to microscopic statistical mechanical descriptions [19–24,8,9]. The classical work by van 't Hoff gives an equilibrium thermodynamic law for macroscopic osmotic pressure in terms of the overall temperature of the system and the difference in concentration of the solute which is confined by a semi-permeable membrane with that of the solute in the outside bulk solvent [24]. A microscopic approach can also be taken based on the mechanics of the solute wall interactions which does not necessarily require the system to be in thermodynamic equilibrium [19,20].

In this paper we shall take a microscopic approach to the study of how the osmotic pressure arises in the non-equilibrium setting of active chemical reactions and fluid flows. We shall then perform analysis to obtain a description of the osmotic pressure of the pump by taking the limit in which the solute confining potentials at the semi-permeable membranes only act in a very small boundary layer of the capping ends of the pump, which corresponds to what we term the “hard-walled limit” [19]. This description is then used to carry out three-dimensional numerical simulations of the microfluidic pumping mechanism using a variant of the finite volume method of [25] and the immersed boundary method [26].

The paper is organized as follows. In Section 2, the pumping mechanism is discussed. To demonstrate the mechanism, a mathematical model of a pump with cylindrical geometry is formulated in Section 3. To obtain an analytically tractable set of equations, reductions are then made to the model in Section 4 and theoretical predictions for the steady-state pumping rate are given. Numerical methods for the full system of equations for the osmotic phenomena which accounts for general confining potentials, the fluid flows, and chemical reactions are presented in detail in Section 5. The specific numerical methods used for the full three-dimensional model of the osmotic pump are then presented and the results of simulations are discussed in comparison to the theoretical predictions made from the reduced model.

2. The pumping mechanism

For concreteness we shall discuss the mechanism in the context of a system which has two solute species A and B which are assumed to be confined to the interior of a cylindrical tube. Two planar cross-sections of the tube are spanned by membranes which are permeable to solvent but impermeable to the solute species A and B . The curved cylindrical walls of the tube are impermeable to solute and solvent alike. For the purpose of our analysis we shall regard the entire cylindrical pump as being embedded in a longer tube which is bent to reconnect with itself so that solvent fluid is re-circulated. We shall assume that this is done in such a manner that the curvature has a negligible effect on the solvent flow. More general geometries and additional solute species could of course be considered to obtain other variants of the proposed pumping mechanism.

The chemistry of the system will occur only in the vicinity of the membranes spanning the cross-section of the tube. Since these membranes act like “caps” for the cylindrical region defined between the cross-sections we shall refer to the semi-permeable membranes as “capping membranes”. The capping membrane at one end of the tube contains reaction sites (embedded enzymes) at which a solute molecule of species B is split into two solute molecules of species A . At the other end of the tube is a capping membrane with embedded reaction sites which combine two molecules of species A to form a single molecule of species B . We remark that even though one of the chemical reactions is the reverse of the other, an energy source is needed to power the pump in general. This is because the chemical reactions are localized and not directly coupled, with one reaction occurring independently at

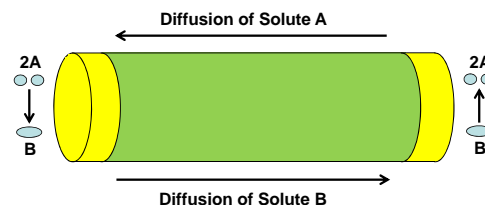


Fig. 2.1. Pump schematic. On the left end of the tube two molecules of species A bind to form a single molecule of species B . When molecules of species B diffuse or are transported by the fluid to the right end of the tube the molecule of species B is split into two molecules of species A . Throughout the chemical reactions the total number of elementary chemical units is conserved as either free species A molecules or as bound pairs which form a single molecule of species B .

one end of the tube, provided there are sufficient reactants, while the other reaction occurs independently at the other end of the tube.

Suppose for example that one of the chemical reactions, say $B \rightarrow A + A$, is strongly favored (for energetic and/or entropic reasons) under the prevailing conditions throughout the pump, and therefore requires only a catalyst to occur. Then no energy source is needed at the capping membrane where this reaction occurs. However, precisely because the $B \rightarrow A + A$ reaction is favored, we cannot expect the reverse reaction $A + A \rightarrow B$ to happen preferentially at the other capping membrane. For the reaction $A + A \rightarrow B$ to occur requires an energy source. In an experimental system the chemistry might be realized by enzymes embedded in the membranes of the capping ends which derive energy from an auxiliary source such as hydrolysis of ATP molecules, see [27]. Another approach to obtain a similar effect as we shall discuss could be to utilize for ions or small molecules a form of “facilitated diffusion” for transport across the capping membranes which has different kinetics for the two membranes [13]. For a schematic of the pumping mechanism see Fig. 2.1.

At steady-state the system is expected to have an imbalance in the number of solute molecules at the opposing ends of the tube. Osmotic pressure differences at the ends of the tube are then expected to drive a fluid flow through the tube from the end with a greater number of solute molecules toward the end with fewer molecules. However, predicting features of this steady-state on intuitive grounds is made challenging given the coupling between the chemical reactions, transport by the fluid, and diffusion. As we shall discuss, the flow may be made to move opposite to the natural direction suggested by the chemical reactions by an appropriate choice of the relative diffusivities of the solute species.

3. A theoretical model of the pump

The geometry of the model system consists of a long tube having total length L and radius R . The pump will be embedded in this long tube and consist of a sub-segment of the tube of length L which is delimited by two semi-permeable membranes. We shall refer to this region as the “tube” of the pump. References to the “ends of the tube” will refer to the boundaries defined by the semi-permeable membranes. Throughout, the pump should be regarded as being embedded within a longer tube of length L which reconnects with itself to re-circulate the solvent fluid, which corresponds to periodic boundary conditions on the tube of length L .

To take into account how osmotic effects arise in the system, explicit solute–wall interactions are modeled through two conservative forces having potentials V_A and V_B , which act on the solute particles of species A and B respectively. To separate those forces acting on the solute inside the tube and those forces acting merely to confine solute particles to the tube, the geometry used in the mathematical model will consist of a slightly larger cylindrical tube having radius R_C and extending in length from T to L_C .

Fig. 3.1. Schematic of the potential energy. The osmotic pump is embedded in a long tube of length L which connects with itself to re-circulate the solvent fluid, this corresponds to periodic boundary conditions on the domain $[0; L]$. In the embedding the interior of the pump extends from $[0; L]$. The potential energy for the confining force is assumed to be non-zero only in a boundary layer of width δ at the capping ends of the tube. A notable feature of the potential is that it is zero at the location of the reaction sites (denoted by boxes) which are modeled by appropriate source and sink terms in Eqs. (3.1) and (3.2). This prevents the confining forces from interfering with the diffusion of solute to these sites. The potential is also assumed to diverge in the boundary layer to prevent solute from diffusing outside the extended tube. We further remark that since all of solute A is converted to B at $x = 0$, solute A does not enter the region $x < 0$, so only the potential V_B is needed there to confine solute B to the tube. Similarly, all of solute B is converted to A at $x = L$, so only the potential V_A is needed for $x > L$ to confine the solute A .

We also define the average flux of concentration over a cross-section by:

$$J_A(x; t) = \frac{1}{R^2} \int_{y^2+z^2 < R^2} \mathbf{j}_A(x; y; z; t) \cdot \mathbf{e}_1 dydz \quad (3.11)$$

$$J_B(x; t) = \frac{1}{R^2} \int_{y^2+z^2 < R^2} \mathbf{j}_B(x; y; z; t) \cdot \mathbf{e}_1 dydz \quad (3.12)$$

and the average fluid velocity by:

$$\mathbf{u}_0(t) = \frac{1}{R^2} \int_{y^2+z^2 < R^2} \mathbf{u}(x; y; z; t) \cdot \mathbf{e}_1 dydz \quad (3.13)$$

In this notation, \mathbf{e}_1 denotes the unit vector in the axial direction (x -direction) and R is the radius of the tube. We remark that from the incompressibility of the fluid flow and the impermeability of the walls to the fluid, the flow is confined to the interior of the tube and is volume conserving, therefore, the average fluid velocity over a cross-section is independent of x .

To obtain a closed system of conservation equations for the cross-sectional concentrations we shall make a number of assumptions and approximations. For the confinement potential for the curved cylindrical boundary of the tube we take the limit of the confinement potential to a hard-wall potential, $V \rightarrow \infty$. In this limit the solute can be handled by no-flux boundary conditions $\mathbf{j}_A(x; y; z; t) \cdot \mathbf{n}_R = \mathbf{j}_B(x; y; z; t) \cdot \mathbf{n}_R = 0$ when $y^2 + z^2 = R^2$, where \mathbf{n}_R is the outward normal in the radial direction. Under this simplification the potentials V_A and V_B appearing in the conservation equations will be used to model only the confinement forces of the solute at the planar boundaries of the tube where the fluid can permeate. We shall also assume that the confinement forces act only in the axial direction at the ends of the tube, and require that $V_A(x; y; z) = V_A(x)$ and $V_B(x; y; z) = V_B(x)$.

To obtain an expression for J_A , and similarly for J_B , we shall approximate the cross-sectional average of the term $\mathbf{u}(x; y; z; t) \cdot \mathbf{e}_1 / C_A(x; y; z; t)$, appearing when (3.3) is substituted into (3.11), by the term $\mathbf{u}_0(t) / C_A(x; t)$. There are two different circumstances in which this would be an especially good approximation. The first is when the tube is sufficiently narrow that $c_A(x; y; z; t)$ is effectively independent of y or z . The second is when the interior of the tube is a porous medium in which case there is a plug flow with a flat velocity profile across a section of the tube so that $\mathbf{u}(x; y; z; t)$ is effectively independent of y and z . In both cases, the vector value \mathbf{u} would have a non-negligible component only in the \mathbf{e}_1 direction since the fluid is incompressible and the tube is straight. A similar set of approximations will also be made for J_B .

With these considerations Eqs. (3.1)–(3.4) can be reduced to the conservation equations:

$$\frac{\partial C_A(x; t)}{\partial t} = - \frac{\partial J_A(x; t)}{\partial x} + \frac{1}{C_A(x; t)} \frac{\partial J_A(x; t)}{\partial x} \cdot \frac{1}{C_A(x; t)} \frac{\partial J_B(x; t)}{\partial x} \cdot \frac{1}{C_B(x; t)} \quad (3.14)$$

$$\frac{\partial C_B(x; t)}{\partial t} = - \frac{\partial J_B(x; t)}{\partial x} + \frac{1}{C_B(x; t)} \frac{\partial J_B(x; t)}{\partial x} \cdot \frac{1}{C_A(x; t)} \frac{\partial J_A(x; t)}{\partial x} \cdot \frac{1}{C_B(x; t)} \quad (3.15)$$

with

$$J_A(x; t) = D_A \frac{\partial C_A(x; t)}{\partial x} - \frac{1}{A} V_A(x; t) C_A(x; t) / C_{A,0}(t) \quad (3.16)$$

$$J_B(x; t) = D_B \frac{\partial C_B(x; t)}{\partial x} - \frac{1}{B} V_B(x; t) C_B(x; t) / C_{B,0}(t) \quad (3.17)$$

where $D_A = D_B = D$, $k_B T = k_B T$, and $\mathbf{u}_0(t)$ is the average velocity. The cross-sectional average velocity of the flow \mathbf{u}_0 , defined in (3.13), will be computed more explicitly in Section 3.1 by assuming a Poiseuille flow [29,30].

The absorbing boundary conditions (3.6), (3.7), and the conservation condition (3.8) extend naturally to the reduced equations, with $C_A(0) = 0$, $C_B(L) = 0$ and

$$\int_0^L C_A(x; t) dx + \int_0^L C_B(x; t) dx = \frac{N_0}{R^2} \quad (3.18)$$

where, as before, N_0 denotes the total number of elementary chemical units. For a schematic of the one-dimensional model and the confining potential, see Fig. 3.1.

At steady-state the equations for $C_A(x)$ and $C_B(x)$ can be solved exactly. In Appendix A, we find the steady-state solution with the general potentials $V_A(x)$ and $V_B(x)$. As mentioned above these potentials are introduced to model explicitly the solute-boundary interactions at the capping ends of the tube confining the solute and will be used mainly to model effects giving rise to osmosis. More details concerning this formulation and how osmotic effects arise will be given in Section 3.2 and Appendix B. An explicit expression for the solute concentrations can be obtained in terms of elementary functions by considering the limit in which the confining potentials at the capping ends become hard-wall potentials, $V \rightarrow \infty$. In this limit the solute concentrations are given by (see Appendix A):

$$C_A(x) = \frac{N_0}{R^2} \exp \left(- \frac{V_A(x)}{k_B T} \right) \exp \left(- \frac{V_B(x)}{k_B T} \right) \quad (3.19)$$

$$C_B(x) = \frac{N_0}{R^2} \exp \left(- \frac{V_B(x)}{k_B T} \right) \exp \left(- \frac{V_A(x)}{k_B T} \right)$$

In the regime $j\bar{u}_0j \ll k_B T = A L$, $j\bar{u}_0j \ll k_B T = B L$ where the transport by the fluid flow is small relative to the diffusivity of the solute molecules, a relatively simple expression can be obtained. By Taylor expanding the exponential terms in (3.19) the steady-state solutions can be approximated by:

$$C_A \cdot x / \frac{2N_0}{R^2 L^2} \frac{A}{C_B} x \quad (3.20)$$

$$C_B \cdot x / \frac{N_0}{R^2 L^2} \frac{B}{C_A} \cdot L \quad x / \quad (3.21)$$

3.1. Approximation of the fluid flow by Poiseuille flow

To model the effective transport of the solute molecules by the fluid flow, we shall use the average velocity of the fluid over a cross-section of the tube, as defined in (3.13). We shall make the approximation that the fluid undergoes a Poiseuille flow inside the tube [29,30].

Consider a cylindrical tube of radius R with a length L that occupies $0 < x < L$ with $y^2 \leq z^2 \leq R^2$. We regard the tube as periodic, i.e., we identify $x \equiv 0$ with $x \equiv L$. Let the part of the tube given by $0 < x < L$ contain the osmotic pump. For reasons related to how osmotic pressure arises from the solute interactions with the confining boundaries, we expect that the presence of the solute will result in an increased pressure inside the region of the tube corresponding to the pump and that there will be pressure differences across the capping membranes which serve as boundaries between the inside and outside of the pump (see Section 3.2). Let these be denoted

$$\cdot 1P_0 \equiv P \cdot 0C / \quad P \cdot 0 \quad / \equiv P \cdot 0C / \quad P \cdot L \quad / \quad (3.22)$$

$$\cdot 1P_L \equiv P \cdot L \quad / \quad P \cdot LC / \quad (3.23)$$

where $P \cdot xC /$ and $P \cdot x \quad /$ denote a pressure at x obtained by a limit from the right or left, respectively. In this case, the $\cdot 1P$ correspond to pressures at the left and right capping ends of the tube of the pump just inside or outside the capping membranes. Note the sign convention that in both cases $\cdot 1P$ is the pressure inside the osmotic pump minus the pressure outside. Thus, we expect both of the $\cdot 1P$ to be positive since the presence of the solute is anticipated to increase the pressure inside the pump relative to the region outside. We remark that the pump corresponds to the segment of the tube from $0; L$ and is embedded in a larger tube from $0; L$ which reconnects with itself to re-circulate the solvent. The periodicity of the larger tube gives that $P \cdot 0 \quad / \equiv P \cdot L \quad /$.

Now we assume Poiseuille flow in both segments of the tube. Since the tube is rigid, and the two segments are in series and have the same radius, this implies that the (linear) pressure gradient is the same in the two segments. Thus

$$G \equiv \cdot P \cdot 0C / \quad P \cdot L \quad / \equiv -L \quad (3.24)$$

$$G \equiv \cdot P \cdot LC / \quad P \cdot L \quad / \equiv -L \quad (3.25)$$

where G is the axial pressure gradient in either of the two segments of the tube. Multiply the first of these equations by L , the second by $\cdot L \quad L /$, and add the results. Making use of the above definitions of $\cdot 1P_0$ and $\cdot 1P_L$, we see that

$$GL \equiv \cdot 1P_0 \quad \cdot 1P_L \quad (3.26)$$

It follows that the effective driving pressure for flow through the entire tube of length L is the difference between the pressure jumps at the capping membranes. In particular, the fluid velocity in either segment of the tube is given by

$$u \cdot x; y; z / \equiv \frac{\cdot 1P_0 \quad \cdot 1P_L}{4 L} R^2 \quad y^2 \quad z^2 \quad e_1 \quad (3.27)$$

and the mean velocity in a cross-section of the tube in either segment is

$$\bar{u}_0 \equiv \frac{\cdot 1P_0 \quad \cdot 1P_L}{8 L} R^2 \quad (3.28)$$

3.2. Pressure at the capping ends: A model of osmotic effects

At the ends of the tube of the pump the solvent fluid molecules are allowed to freely permeate the capping membranes while the solute particles interact with the membrane and are restricted to remain in the interior of the pump. As a consequence of these solute membrane interactions and the solute solvent interactions, a fluid pressure arises from the confinement of the solute particles, which is generally referred to as "osmotic pressure" [19].

To obtain the pressures $\cdot 1P_0$ and $\cdot 1P_L$ for the proposed pumping mechanism, we must consider the non-equilibrium setting. In Appendix B we discuss the non-equilibrium pressures which arise when taking into account both the role of the chemical reactions and fluid flow. We then consider the limit as the potential becomes "hard-walled", in the sense that the solute interacts with the confining walls only over a very small boundary layer. In this case, it is found that for the non-equilibrium steady-state of the pump the van 't Hoff's Law [24] holds in a local sense at the capping ends of the tube. This gives for the pressures:

$$\cdot 1P_0 \equiv k_B T C \cdot 0C / \quad (3.29)$$

$$\cdot 1P_L \equiv k_B T C \cdot L \quad / \quad (3.30)$$

where $C \cdot x / \equiv C_A \cdot x / C_B \cdot x /$ is the average concentration of solute particles in a cross-section of the tube at axial coordinate x . We remark that from the absorbing boundary conditions (3.6), (3.7) at the capping ends, this can be simplified by using that the concentrations reduce to $C \cdot L / \equiv C_A \cdot L /$ and $C \cdot 0 / \equiv C_B \cdot 0 /$.

4. Theoretical predictions for the steady-state pumping rate

To predict the steady-state pumping rate, the equations for the solute concentration must be coupled to the fluid flow. This can be done by assuming that the fluid is pumped as a Poiseuille flow having pressures at the ends of the tube given by the local van 't Hoff's Law discussed in Sections 3.1 and 3.2. This gives for the average velocity of the fluid over a cross-section of the tube:

$$\bar{u}_0 \equiv \frac{R^2 k_B T}{8 L} \cdot C_A \cdot L / \quad C_B \cdot 0 / \quad (4.1)$$

By substituting the steady-state solutions (3.19) for the solute concentrations into (4.1), the following nonlinear equation is obtained:

$$\bar{u}_0 \equiv \frac{N_0 k_B T}{8 L} \frac{h \exp \frac{A \bar{u}_0}{k_B T} L}{\exp \frac{A \bar{u}_0}{k_B T} L} \frac{1}{1} \frac{h}{\frac{1}{2}} \frac{1}{\exp \frac{B \bar{u}_0}{k_B T} L} \frac{1}{\exp \frac{B \bar{u}_0}{k_B T} L} \quad (4.2)$$

While finding an analytic expression for the solution of the nonlinear equation (4.2) is not possible the equations can be readily solved using a numerical method such as Newton iteration [31]. To obtain approximate analytic expressions for \bar{u}_0 , we shall consider the asymptotic regime $j\bar{u}_0j \ll k_B T = A L$, $j\bar{u}_0j \ll k_B T = B L$ which allows for linearization of (4.2). The asymptotic results will then be compared with numerical solutions of (4.2) and numerical simulations of a three-dimensional model of the pump. The parameters used throughout are given in Table C.2.

In the regime where $j\bar{u}_0] \quad k_B T = A L, j\bar{u}_0] \quad k_B T = B L$, we can solve for \bar{u}_0 by Taylor expanding the exponential terms in (4.2) to obtain:

$$\bar{u}_0 = \frac{N_0 k_B T}{8 L L} - \frac{B}{A} \frac{2}{C} \frac{A}{B} \quad (4.3)$$

We remark that this can also be found by substituting the approximate expressions (3.20) and (3.21) for the solute concentrations into (4.1).

The steady-state volumetric pumping rate is then given by:

$$Q = \frac{R^2 \bar{u}_0}{8 L L} = \frac{N_0 k_B T R^2}{8 L L} - \frac{B}{A} \frac{2}{C} \frac{A}{B} \quad (4.4)$$

From these expressions a number of interesting features of the pump are suggested. Letting $D_A = D_B$ in (4.4) the dependence of the pumping rate on the drag coefficients can be expressed as:

$$Q = \frac{N_0 k_B T R^2}{8 L L} - \frac{1}{1} \frac{2}{C} \quad (4.5)$$

One feature of this regime is that the pumping rate depends on the geometry of the pump through the ratio $R^2 = L L$. $D_A = D_B$ in (4.4) the dependence of the pumping rate on the drag coefficients can be expressed as: which shows a dependence on the "shape" of the system but not the size. The "shape" of the system characterizes the aspect ratio of the tube of the pump and the fraction the pump comprises of the tube of total length L . We remark that this conclusion is for a fixed number of elementary solute units N_0 , however. If N_0 scales linearly with the volume of the tube, as one might reasonably expect, then the pump flow Q (volume/time) will also scale linearly with the volume of the tube, provided the "shape" of the system does not change, which is characterized by holding $R^2 = L L$ constant.

A general feature of the pump predicted by this expression is that the direction in which fluid is pumped is controlled by the ratio of the drag coefficients. It follows from (4.5) that when $\frac{D_B}{D_A} > \frac{1}{2}$, fluid flows at steady-state from the right capping end, where the paired solute molecules are split, to the left capping end, where the solute molecules are joined into pairs. This is intuitively expected given the stoichiometry of the chemistry and the equilibrium van 't Hoff's Law for osmosis [24]. However, the theoretical results predict that the direction of flow can be reversed by taking $\frac{D_B}{D_A} < \frac{1}{2}$. In this case molecules of species B have a drag coefficient more than double that of molecules of species A and fluid flows from the capping end where the solute molecules are joined into pairs toward the end where the pairs of solute molecules are split. When $\frac{D_B}{D_A} = \frac{1}{2}$ no net flow is predicted to be driven by the pump. For a comparison of the asymptotic expression (4.5) and the pumping rate obtained from numerical solution of (4.2), see Fig. 4.1.

Obtaining flow from left to right may seem counter-intuitive, since the splitting reaction would seem to have the effect of increasing the number of molecules at the right capping end. However, a further consideration must be taken into account and this dramatically affects the flow direction. From (3.20) and (3.21) we see that the greater drag coefficient of species B has the effect of solute persisting longer in the form of molecules of species B as opposed to molecules of species A . As a consequence, there is a relative build up of species B molecules which interact with the left boundary of the tube causing through osmotic effects a left to right fluid flow in the tube. One way species B molecules can become more plentiful at the left end relative to species A at the right end at steady-state, is for molecules of species A to diffuse sufficiently fast against the flow to repopulate the species B molecules being relatively slowly transported by the flow to be split. The analysis shows that $\frac{D_B}{D_A} < \frac{1}{2}$ is sufficient for this to occur.

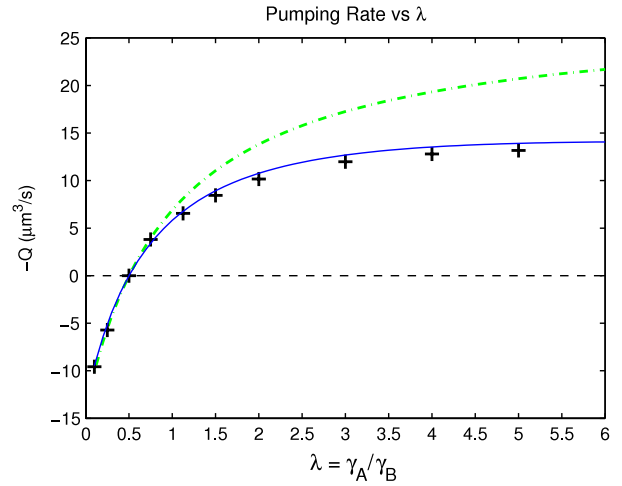


Fig. 4.1. Pumping rate vs λ . A comparison between the theoretical predictions obtained by solution of (4.2) (solid curve), asymptotic expression (4.4) (upper dotted curve), and numerical simulations of the three-dimensional model described in Section 5 (data points). This shows that the one-dimensional theory does a good job of quantitatively predicting the flow rates obtained in the three-dimensional model. To vary the parameter γ_A was adjusted while γ_B was held fixed at the value given in Table C.2. Note that the negative pumping rate is given in the plots.

We remark that if we assume that both species of solute molecules A and B are spherical and have the same mass per unit volume, then, since each molecule of B is comprised of two molecules of A , we have

$$2m_A D_B = 2^{1/3} r_A D_B = 2^{1/3} A D_B \quad (4.6)$$

where m_A, m_B are the masses and r_A, r_B are the radii of the individual solute molecules A and B , respectively, and where we have used the Stokes drag formula, which tells us that the drag coefficient of a sphere is proportional to its radius r . It follows that

$$D_B \frac{A}{B} D_B^{1/3} > 1 = 2: \quad (4.7)$$

In this special case, expression (4.5) reduces to

$$Q = \frac{N_0 k_B T R^2}{16 L L} - \frac{1}{1} \frac{2^{2/3}}{C} \frac{2^{1/3}}{2} \quad (4.8)$$

and the flow goes in the "normal" direction, i.e., from the end of the tube where the dimer B is split toward the end where B is reassembled independent of how the other parameters are chosen. As a result, in order to reverse the flow, as discussed above, we need to increase sufficiently the drag coefficient of B relative to that of A , e.g., by choosing a solute B that adopts an extended floppy conformation when whole, but whose halves A adopt a more spherical conformation after B has been split.

When using (4.5) to predict behaviors of the pump it is important to keep in mind that conclusions drawn from that expression are only strictly valid for parameters in the asymptotic regime $j\bar{u}_0] \quad k_B T = A L, j\bar{u}_0] \quad k_B T = B L$. To further explore the behavior of the pump, numerical solutions were computed for (4.2) over a range of γ_A and γ_B values, see Fig. 4.3.

A qualitative feature of the pump suggested by (4.5) is that as the drag coefficients of the solute molecules are taken large, the pumping rate remains bounded. The numerical solutions also support this conclusion, see Fig. 4.3. The structure of the level curves in Fig. 4.3 indicate that the pumping rate converges to zero in the limit of large drag coefficients when the ratio λ is held fixed. For a fixed drag coefficient such as γ_A the level curves indicate that there is an optimal choice for the other drag coefficient γ_B which maximizes the pumping rate. The numerical results also

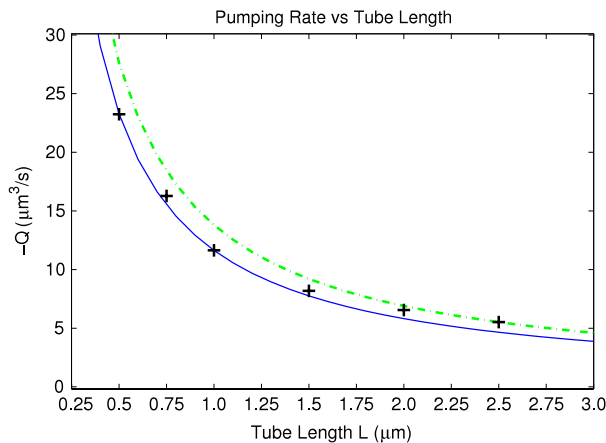


Fig. 4.2. Pumping rate vs L . The theoretical prediction for the steady-state pumping rate obtained by numerical solution of (4.2) (solid curve) and the asymptotic expression (4.8) (dashed curve) is compared to the results obtained by simulating the three-dimensional model of the pump described in Section 5 (data points). Note that the negative pumping rate is given in the plots.

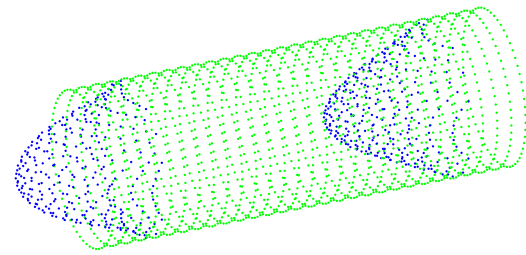


Fig. 5.1. Steady-state fluid flow for the three-dimensional pump model. Tracer particles are distributed across a cross-section of the tube and are swept along with the flow as immersed boundary method control points are plotted (blue). The control points which model the tube boundary impermeable to both the fluid and solute molecules are plotted (green). The fluid flow appears to be approximately Poiseuille. (For interpretation of the references to colour in this figure legend, the reader is referred to the web version of this article.)

between the predictions of the one-dimensional model and the results of the three-dimensional simulations, see Figs. 4.1 and 4.2.

5.1. The immersed boundary method for the fluid

The natural scale for the pumps we shall consider is at most a few hundred microns in length. For concreteness, we shall restrict ourselves to modeling pumps immersed in water at room temperature. For such systems, the Reynolds number is quite small allowing for the fluid flow to be described to a good approximation by the incompressible Stokes equations:

$$\frac{\partial \mathbf{u}(\mathbf{x}; t)}{\partial t} + \nabla \cdot (\mathbf{u} \otimes \mathbf{u}) = -\nabla p + \nabla^2 \mathbf{u} + \mathbf{f}(\mathbf{x}; t) \quad (5.1)$$

$$\nabla \cdot \mathbf{u} = 0 \quad (5.2)$$

where \mathbf{u} is the velocity of the fluid, ρ is the density of the fluid, η is the dynamic viscosity of the fluid, p is the pressure, and \mathbf{f} is a forcing term.

In the immersed boundary method [26] the forcing term \mathbf{f} is introduced to model structures interacting with the fluid. In practice, the structures are discretized and represented by a collection of elementary control points. The dynamics of the collection of control points and the manner in which corresponding forces are handled is given by:

$$\mathbf{f}(\mathbf{x}; t) = \sum_{j \in \mathcal{D}} \mathbf{F}^{(j)}(\mathbf{x}) \cdot \mathbf{X}^{(j)}(t) / \Delta \quad (5.3)$$

$$\frac{d\mathbf{X}^{(j)}(t)}{dt} = \mathbf{u}(\mathbf{x}^{(j)}; t) \quad (5.4)$$

where $\mathbf{X}^{(j)}$ is the position of the j th particle, $\mathbf{F}^{(j)}$ is the force acting on the j th particle, and Δ is a weight function which integrates to one and is non-zero only on a region centered at the origin and having diameter equal to Δ .

In the immersed boundary method the structures are treated essentially as part of the fluid. Forces that act on a particle are transmitted directly to the fluid through the weight function $\Delta(\mathbf{x} - \mathbf{X}^{(j)})$. The particles move at a velocity determined by averaging with the weight function Δ the fluid velocity locally in a neighborhood of the particle. For a further discussion see [26] (See Fig. 5.1).

To obtain numerical methods for the immersed boundary equations, the system is discretized in space on a uniform periodic mesh using the standard central difference approximation for the Laplacian and discretized in time using the Forward-Euler method:

$$\frac{\mathbf{u}_m^{n+1} - \mathbf{u}_m^n}{\Delta t} = -\nabla \cdot (\mathbf{u}_m^n \otimes \mathbf{u}_m^n) - \nabla p_m^n + \nabla^2 \mathbf{u}_m^n + \mathbf{f}_m^n \quad (5.5)$$

Fig. 4.3. Pumping rate vs A and B . The theoretical predictions for the pumping rate obtained by numerical solution of (4.2) as both A and B are varied. The colors indicate the magnitude and direction of the pumping rate as indicated in the color bar to the right, where a positive rate indicates pumping from right to left. The gray lines denote level curves of the pumping rate. The dark line indicates the level curve corresponding to a pumping rate of zero. This line separates the two directions in which the fluid is driven by the pump with the region below this line corresponding to pumping from right to left and the region above corresponding to pumping from left to right.

show that as the drag coefficients are taken small the pumping rate dramatically increases. This behavior is somewhat expected on intuitive grounds as the smaller drag coefficient increases the diffusive rate of turnover in the chemical reactions.

5. Numerical methods for the three-dimensional pump model

In the one-dimensional model a number of approximations were made to obtain an analytically tractable set of equations. In order to investigate further the behaviors of the pump indicated by the one-dimensional analysis, we shall numerically simulate the full three-dimensional model incorporating both the solute concentration fields and the steady-state dynamics of the fluid. The simulations are performed using an extension of the immersed boundary method which handles the solute concentration fields through a finite volume method. Details of the numerical method are discussed in the following two sections. For a comparison

Fig. 5.2. Schematic of the three-dimensional pump model. The immersed boundary method control points used to model the cylindrical boundary which is impermeable to both the fluid and solute molecules are plotted (green). The cubic cells of the finite volume method are shown in the interior of the tube (gray). The cells participating in the chemical reactions for the splitting reaction are on the right end of the tube (yellow) and the cells for the binding reaction are on the left end of the tube (yellow). (For interpretation of the references to colour in this figure legend, the reader is referred to the web version of this article.)

where \mathbf{u}_m^n denotes the velocity value at the grid point with index $\mathbf{m} \in \{m_1; m_2; m_3\}$ at the time step with index n corresponding to the time $t_n \in [n-1]t, n]$. For N grid points in each direction we have $1x \in [L-1]N$. The term \mathbf{e}_q denotes the standard basis vector which has a value of 1 in the q th component and 0 in all other components. The term \mathbf{f}_m^n denotes the force at the \mathbf{m} th grid point for the n th time step.

In (5.5) the incompressibility constraint (5.2) is handled by the operator \mathcal{P} determined by the projection method [32]. The projection operator is derived from the “principle of virtual work” for the discrete divergence constraint:

$$\sum_{q \in \{1\}} \frac{\mathbf{u}_m^n \cdot \mathbf{e}_q}{1x} = 0; \quad (5.6)$$

The projection operator can be expressed as:

$$\mathcal{P} \mathbf{u}_m = \sum_{\mathbf{k}} \hat{\mathcal{P}}_{\mathbf{k}} \hat{\mathbf{u}}_{\mathbf{k}} e^{i2\pi \mathbf{k} \cdot \mathbf{m}/N} \quad (5.7)$$

where $\hat{\mathbf{u}}_{\mathbf{k}}$ denotes the Discrete Fourier Transform (DFT) of the velocity field \mathbf{u}_m , and

$$\hat{\mathcal{P}}_{\mathbf{k}} = \frac{\hat{\mathbf{g}}_{\mathbf{k}} \hat{\mathbf{g}}_{\mathbf{k}}^T}{|\hat{\mathbf{g}}_{\mathbf{k}}|^2} \quad (5.8)$$

where \mathbf{I} is the identity matrix and

$$\hat{\mathbf{g}}_{\mathbf{k}}^{(q)} = \sin(2\pi \mathbf{k} \cdot \mathbf{q}/N) = 1x; \quad (5.9)$$

In this notation the parenthesized superscript q denotes the vector component. The projector operator \mathcal{P} and the terms $\hat{\mathbf{g}}_{\mathbf{k}}$ can be derived by taking the DFT of the incompressibility condition (5.6), which becomes $\hat{\mathbf{g}}_{\mathbf{k}} \cdot \hat{\mathbf{u}}_{\mathbf{k}} = 0$.

The equations of the fluid–structure coupling become:

$$\begin{aligned} \mathbf{f}_m^n &= \sum_{j \in \{1\}} \mathbf{F}^{(j)}_{a, \mathbf{x}_m} \mathbf{x}_m^{(j)} / \\ &= \frac{\mathbf{x}_m^{(1)} \cdot \mathbf{x}_m^{(j)}}{1t} = \sum_{\mathbf{m}} \mathbf{a} \cdot \mathbf{x}_m \mathbf{x}_m^{(j)} / \mathbf{u}_m^n 1x^3; \end{aligned}$$

To model the impermeable boundary of the pump a collection of control points is distributed over the curved surface of the cylinder. Each control point is then targeted to a point on the cylinder with the linear restoring force:

$$\mathbf{F}^{(j)} = -K \mathbf{x}_0^{(j)} - \mathbf{x}_0^{(j)}$$

where the $\mathbf{x}_0^{(j)}$ denotes the specific target points on the surface of the cylinder indexed by j . By choosing a sufficiently large stiffness

K and density of control points the curved boundary of the cylinder is to a good approximation impermeable to fluid. See Fig. 5.2 for a schematic of the pump model.

While other methods can be used to solve for Stokes flow in a cylindrical tube the implementation of the immersed boundary method has the potential of being amenable to simulations involving complicated geometries and/or elastic boundaries. To model such a boundary a mesh of control points could again be arranged over the surface of the cylinder, but instead of targeting control points to specific locations in space they could be linked to each other by linear springs with non-zero rest lengths or indeed by nonlinear springs. In principle, more general geometries and models could be studied with these methods, such as the role of fluid flow in the osmotic swelling of semi-permeable immersed structures.

5.2. The finite volume method for the solute concentration field

In this section we discuss the evolution of the concentration fields of the solute. A finite volume method is developed for Eqs. (3.1)–(3.4) in which the three-dimensional spatial domain is subdivided into N^3 cubic cells. To model the evolution of the concentration field, fluxes are determined for the exchange of solute between the cells. In the model the role of the conservative forces, diffusion, and advective transport of the solute concentration by the fluid are taken into account.

We shall use the following finite volume discretization:

$$\begin{aligned} c_{n, \mathbf{C}1, \mathbf{m}}^A &= c_{n, \mathbf{m}}^A \\ &= \frac{1}{2} \sum_{\mathbf{q} \in \{1\}} \sum_{\mathbf{m}} \left(\frac{A, B}{\mathbf{m}} \right) \times \frac{A, \mathbf{q} c_{n, \mathbf{q}}^A 1t}{\mathbf{q}^2 \mathbf{m}} \times \frac{A, \mathbf{q} c_{n, \mathbf{m}}^A 1t}{\mathbf{q}^2 \mathbf{m}} \\ &= \frac{1}{2} \sum_{\mathbf{q} \in \{1\}} \sum_{\mathbf{m}} \left(\frac{B, A}{\mathbf{m}} \right) \times \frac{B, \mathbf{q} c_{n, \mathbf{q}}^B 1t}{\mathbf{q}^2 \mathbf{m}} \times \frac{B, \mathbf{q} c_{n, \mathbf{m}}^B 1t}{\mathbf{q}^2 \mathbf{m}} \end{aligned} \quad (5.10)$$

$$\begin{aligned} c_{n, \mathbf{C}1, \mathbf{m}}^B &= c_{n, \mathbf{m}}^B \\ &= \frac{1}{2} \sum_{\mathbf{q} \in \{1\}} \sum_{\mathbf{m}} \left(\frac{A, B}{\mathbf{m}} \right) \times \frac{A, \mathbf{q} c_{n, \mathbf{q}}^A 1t}{\mathbf{q}^2 \mathbf{m}} \times \frac{A, \mathbf{q} c_{n, \mathbf{m}}^A 1t}{\mathbf{q}^2 \mathbf{m}} \\ &= \frac{1}{2} \sum_{\mathbf{q} \in \{1\}} \sum_{\mathbf{m}} \left(\frac{B, A}{\mathbf{m}} \right) \times \frac{B, \mathbf{q} c_{n, \mathbf{q}}^B 1t}{\mathbf{q}^2 \mathbf{m}} \times \frac{B, \mathbf{q} c_{n, \mathbf{m}}^B 1t}{\mathbf{q}^2 \mathbf{m}} \end{aligned} \quad (5.11)$$

where $1t$ denotes the time step, $c_{n, \mathbf{m}}^A$ denotes the concentration of solute species A at time n in the cell with index \mathbf{m} , with a similar interpretation for species B , and \mathbf{m} is the set of indices for the neighbors of cell \mathbf{m} in the Cartesian directions. The factor $\frac{A, \mathbf{q}}{\mathbf{m}}$ is the rate that concentration of species A leaves cell \mathbf{m} and enters cell \mathbf{q} , with a similar interpretation for species B (see Fig. 5.3). The factors $\frac{A, B}{\mathbf{m}}$ and $\frac{B, A}{\mathbf{m}}$ model the chemical reactions and are defined by:

$$\frac{A, B}{\mathbf{m}} = \begin{cases} 1; & \text{if } m_1 \in m_1^0 \\ 0; & \text{otherwise} \end{cases} \quad (5.12)$$

and

$$\frac{B, A}{\mathbf{m}} = \begin{cases} 1; & \text{if } m_1 \in m_1^L \\ 0; & \text{otherwise} \end{cases} \quad (5.13)$$

where $\mathbf{m} \in \{m_1; m_2; m_3\}$, m_1^0 is the index corresponding to the cross-section of the tube at $x \in 0$ near the left end of the tube, and m_1^L is the index corresponding the cross-section at $x \in L$. To account for the situation in which the chemical reactions process all available reactants in the cell, absorbing boundary conditions are imposed with $c_{n, m_1^0; m_2; m_3}^A = 0$ and $c_{n, m_1^L; m_2; m_3}^B = 0$.

Fig. 5.3. Finite volume method. Depicted are the mesh cells of the finite volume method used to account for the concentrations of the chemical species. The terms correspond to the fluxes of concentration which occurs through each of the cell faces. The terms correspond to exchanges which occur between the mesh cells involved in the splitting and binding reactions.

In Eqs. (3.1)–(3.4) the solute concentration is subject to diffusion, drift by conservative forces, and transport by the fluid. For the concentration of species A this is taken into account using the following rates of exchange between the cells:

$$\dot{c}_{m,q}^A \approx \frac{D_A}{\Delta x^2} \exp\left(\frac{V_{m,q}^A}{k_B T}\right) \left(c_{m,q}^A - c_{m,m}^A \right) + \dot{u}_{m,q}^n \frac{1}{\Delta x} \quad (5.14)$$

where Δx denotes the grid spacing between the center of adjacent cells, D_A denotes the diffusion coefficient of the solute, and

$$\dot{u}_{m,q}^n \approx \frac{V_{m,q}^A - V_m^A}{k_B T} \quad (5.15)$$

and

$$\dot{u}_{m,q}^n \approx \max(\mathbf{u}_{m,q}^n \cdot \mathbf{e}_{m,q}; 0) \quad (5.16)$$

The fluid velocity $\mathbf{u}_{m,q}^n$ is obtained from the fluid velocity field of Eq. (5.5) by an interpolation to the cell faces:

$$\mathbf{u}_{m,q}^n \approx \frac{1}{2} (\mathbf{u}_m^n + \mathbf{u}_q^n) \quad (5.17)$$

The first term in the rate equation (5.14) follows the derivation in [25] and has desirable properties with respect to the equilibrium distribution of the solute, which is discussed below. The second term in (5.14) is added to account for the advection of the solute by the fluid. The factor $\dot{u}_{m,q}^n$ is the positive component of the velocity in the direction $\mathbf{e}_{m,q}$ given by the vector from the center of the cell with index m to the center of the cell with index q . This ensures that the exchange rates are always positive and that in the absence of force or diffusion a cell receives concentration only from cells located “upwind” with respect to the velocity field. A similar set of rates using the potential V_B is used for the solute concentration of species B .

It can be readily checked that the scheme (5.10)–(5.16) is conservative. Further, it can be shown in the absence of the chemical reactions, when $\dot{c}_m^{A,B} \approx 0 \approx \dot{c}_m^{B,A}$ for all m , and transport by the fluid, when $\mathbf{u}_m \approx 0$, that detailed balance, in which there is no net exchange of solute between cells, holds for the distribution:

$$c_m^A \approx \frac{1}{Z} \exp\left(-\frac{V_m^A}{k_B T}\right) \quad (5.18)$$

where

$$Z \approx \sum_m \exp\left(-\frac{V_m^A}{k_B T}\right) \Delta x^3 \quad (5.19)$$

This concentration corresponds to the thermodynamic equilibrium associated with non-interacting particles subject to a conservative

force with potential $V_A \cdot \mathbf{x}/\Delta x$ restricted to lattice sites \mathbf{x}_m . Thus the steady-state of the numerical method without chemical reactions and transport by the fluid corresponds exactly to an equilibrium distribution. A similar result holds for the species B equations.

To couple the fluid equations to the solute concentration fields the following force density is introduced in (5.5):

$$\mathbf{f}_{\text{sol},m}^n \approx \left(\frac{V_A \cdot \mathbf{x}_m}{\Delta x} c_{n,m}^A - \frac{V_B \cdot \mathbf{x}_m}{\Delta x} c_{n,m}^B \right) \mathbf{n}_m \quad (5.20)$$

which transmits the force acting on the solute molecules within a given cell directly to the fluid.

5.3. Conditions imposed for the pump with hard-wall confining potential

In the hard-walled confining potential limit, where the length scale of the solute–wall interactions becomes very small $\Delta x \rightarrow 0$, the explicit force acting on the solute can be replaced with zero flux boundary conditions. In the finite volume method this corresponds to setting $\dot{c}_{m,q}^A \approx 0$ for all cells with index q lying outside of the tube, see Fig. 5.2. In this limit the osmotic effects in the model are taken into account using the local van ’t Hoff law derived in Appendix B. In particular, for the cells adjacent to the planar boundaries of the tube the force acting on the fluid arising from the solute–wall interactions is then given by:

$$\mathbf{f}_{\text{sol},m}^n \approx c_{n,m} k_B T \frac{1}{\Delta x^2} \mathbf{n}_m = \frac{1}{\Delta x^3} \quad (5.21)$$

where $c_{n,m} \approx c_{n,m}^A + c_{n,m}^B$ and \mathbf{n}_m is the inward normal of the boundary.

For a schematic of the three-dimensional pump model see Fig. 5.2. In Figs. 4.1 and 4.2 numerical simulations of the three-dimensional pump model are compared with the theoretical predictions.

6. Conclusions

A basic mechanism has been shown by which chemical reactions can be used to generate osmotic pressure gradients which drive fluid flows. A specific pumping mechanism was discussed in which two solute species diffuse and undergo basic chemical reactions at opposite ends of a tube, where one reaction splits solute molecules while the other fuses together solute molecules. In contrast to other osmotically driven systems, the mechanism presented here does not rely on an external store of solute molecules. Instead, the process which sets up the osmotic pressure gradient recycles the solute molecules through the two reversible chemical reactions.

To study the non-equilibrium steady-state behavior of the pumping mechanism, theoretical models were formulated which self-consistently take into account the diffusion of the solute species, advective transport by the fluid flow, chemical reactions, and interactions with the confining walls. The analytic results and numerical simulations demonstrate that the osmotic pump is capable of driving a fluid flow in either direction through the tube by an appropriate choice of the relative diffusivities of the solute molecules, while retaining the same chemical kinetics at the capping membranes.

Many variants of the proposed pumping mechanism can be considered. One possible variant would be to utilize at the membrane boundaries additional chemical reactions in which more intermediate products and reactants are involved. For instance, this could be utilized to control the response of the pump to external signaling molecules which turn the pump on or off or change the preferred direction of fluid flow. Such reactions could also potentially be designed to provide a feedback mechanism which depends on the rate of fluid flow, or introduces additional

time scales into the physical system allowing for oscillatory behaviors in which the pump turns on or off or reverses direction periodically. In the biological context such chemical kinetics would be expected to play an important role in regulating the behavior of osmotic pumps. For example, in a hypothetical mechanism of cell motility involving such osmotic pumps embedded in the cell membrane, such an oscillatory behavior could play a constructive role by coordinating the propulsion generated by multiple pumps and such an ability to turn pumps on or off locally could be used in cell motility to control speed and direction.

Other variants of the proposed pumping mechanism could also be considered in which the geometry of the confining region is varied to have different shapes which are static or change dynamically in response to the osmotic pressures, fluid flow, and solute concentrations. It is expected that such systems could be designed to exhibit a rich variety of features making use of the geometry dependent feedback the fluid flow has on the diffusivity of solute molecules and osmotic pressures generated. The analytic and numerical techniques introduced in this work offer one approach to investigate such osmotically driven systems.

Acknowledgements

The authors would like to thank Peter R. Kramer for stimulating conversations concerning non-equilibrium systems. The authors would also especially like to thank George Oster, whose vision of direct modeling of osmotic phenomena inspired this line of research. The author P.J.A. was supported by (NSF DMS - 9983646 and NSF DMS-0635535).

Appendix A. General solution of the steady-state solute concentrations

The equations for the solute concentrations will now be solved in the steady-state when the solute molecules are subject to a flow u_0 and conservative forces $- \nabla V_A$, $- \nabla V_B$, for species A and B respectively.

For computational convenience we remark that equations (3.14) and (3.15) can be expressed in a form involving the divergence (in one dimension $\partial/\partial x$) of purely flux-like terms:

$$\frac{\partial C_A \cdot x / t}{\partial t} = \frac{\partial J_A \cdot x / t}{\partial x} \quad (A.1)$$

$$\frac{\partial C_B \cdot x / t}{\partial t} = \frac{\partial J_B \cdot x / t}{\partial x} \quad (A.2)$$

with

$$J_A \cdot x / t = J_A \cdot 0^C / t \cdot x / 1 + 2 J_B \cdot L / t \cdot x / L \quad (A.3)$$

$$J_B \cdot x / t = J_B \cdot 0^C / t \cdot x / 1 + C J_B \cdot L / t \cdot x / L \quad (A.4)$$

where J_A and J_B are defined in (3.16) and (3.17). In this notation $x /$ denotes the Heaviside function defined by:

$$x / = \begin{cases} 0; & \text{if } x < 0 \\ 1; & \text{if } x \geq 0 \end{cases} \quad (A.5)$$

The steady-state of Eqs. (3.14)–(3.17) requires that the fluxes be constant:

$$J_A \cdot x / = J_A^0 \quad (A.6)$$

$$J_B \cdot x / = J_B^0 \quad (A.7)$$

where J_A^0 and J_B^0 are arbitrary constants to be determined. We remark that the constants J_A^0 and J_B^0 can be interpreted as the steady-state fluxes of each of the solute species A and B, respectively. From this, (A.3), (A.4), and the definition of the fluxes given in (3.16) and (3.17) it follows by the method of integrating factors that:

$$J_A \cdot 0^C / D = J_A^0 \quad (A.8)$$

$$J_B \cdot L / D = J_B^0 \quad (A.9)$$

From (3.16) and (A.6) it then follows that:

$$\frac{\partial}{\partial x} \exp \left(\frac{V_A \cdot x /}{k_B T} \right) C_A \cdot x / = D \frac{1}{D_A} J_A^0 C_A^0 \cdot x / + \frac{1}{D_A} C_A \cdot x / \exp \left(\frac{V_A \cdot x /}{k_B T} \right) \quad (A.10)$$

where the Einstein relations $D_A = k_B T / \zeta_A$, $D_B = k_B T / \zeta_B$ have been used [10,22]. This can be integrated to obtain:

$$C_A \cdot x / = D q_A \cdot x / + J_A^0 / C_A^0 \cdot x / + J_B^0 / C_B^0 \cdot x / \quad (A.11)$$

where

$$q_A \cdot x / = J_A^0 / D \exp \left(\frac{V_A \cdot x /}{k_B T} \right) \quad (A.12)$$

$$A \cdot x / = D \frac{1}{D_A} \int_0^x \frac{y / q_A \cdot x /}{y / dy} \quad (A.13)$$

$$A \cdot x / = D \frac{2}{D_A} \int_0^x \frac{y / L / q_A \cdot x /}{y / dy} \quad (A.14)$$

A similar calculation can be performed to obtain:

$$C_B \cdot x / = D q_B \cdot x / + J_B^0 / C_B^0 \cdot x / + J_A^0 / C_A^0 \cdot x / \quad (A.15)$$

where

$$q_B \cdot x / = J_B^0 / D \exp \left(\frac{V_B \cdot x /}{k_B T} \right) \quad (A.16)$$

$$B \cdot x / = D \frac{1}{2 D_B} \int_0^x \frac{y / q_B \cdot x /}{y / dy} \quad (A.17)$$

$$B \cdot x / = D \frac{1}{D_B} \int_0^x \frac{y / L / q_B \cdot x /}{y / dy} \quad (A.18)$$

The general solution has four unknown constants J_A^0 , J_B^0 , C_A^0 , C_B^0 . To determine these constants the conditions (3.6)–(3.8) will be used. This, however, only gives three conditions for four unknowns. To obtain a fourth condition we shall assume that the confining potentials V_A and V_B grow at a sufficient rate so that $C_A \cdot x / \rightarrow 0$ as $x \rightarrow 1$ and $C_B \cdot x / \rightarrow 0$ as $x \rightarrow 1$. As a consequence, we have that $J_A \cdot x / \rightarrow 0$ as $x \rightarrow 1$ and $J_B \cdot x / \rightarrow 0$ as $x \rightarrow 1$. From (A.6)–(A.9) this gives a fourth condition:

$$J_A^0 = 2 J_B^0 \quad (A.19)$$

This condition can be motivated physically by considering the total flux of mass, including both molecules of species A and B, that passes through a cross-section of the tube, say at the midpoint. Since the solute molecules are confined to the tube and recycled by the chemical reactions the total flux of mass across any interior cross-section at steady-state must be zero, which requires $J_A = C J_B = 0$.

The four conditions can be expressed as a linear system of equations as given in Box 1.

Further simplifications can be made by a judicious choice of x_A^0 and x_B^0 . Setting $x_A^0 = 0$ and $x_B^0 = L$ we obtain $C_A \cdot x_A^0 / = 0 = C_B \cdot x_B^0 /$. This allows for Box 1 to be readily solved in terms of the matrix

Table C.1

Description of the parameters.

Parameter	Description
k_B	Boltzmann's constant
T	Temperature
	Fluid dynamic viscosity
	Fluid density
N_0	Total number of elementary chemical units
C_0	Total concentration of elementary chemical units
L	Length of the tube of the pump
L	Total length of the tube in which the pump is embedded
R	Radius of the tube of the pump
A	Drag coefficient of a molecule of species A
B	Drag coefficient of a molecule of species B

Table C.2

Parameter values (unless otherwise specified).

Parameter	Description
T	300 K
	$6.0221 \cdot 10^5 \text{ amu} \cdot \text{nm} / \text{ns}$
	$602.2142 \text{ amu} \cdot \text{nm}^3$
N_0	1000
L	2000 nm
L	3000 nm
R	400 nm
A	$1.1351 \cdot 10^7 \text{ amu} \cdot \text{ns}$
B	$1.1351 \cdot 10^7 \text{ amu} \cdot \text{ns}$

$O(\cdot)$ denotes the usual order condition that the $jg(x)/C$ where C is a constant [33]. Similarly we have

$$p(L)/D \sim C \cdot L/k_B T \cdot C \cdot O(\cdot) \quad (B.11)$$

Now one could similarly compute the body force and effective pressure for a similar boundary layer just outside the tube at the capping membranes. In the hard-wall limit this would give a difference in the effective pressures across the capping membrane which is proportional to the concentration difference. In particular,

$$[p(0)] \sim D \cdot k_B T \cdot [C(0)] \quad (B.12)$$

$$[p(L)] \sim D \cdot k_B T \cdot [C(L)] \quad (B.13)$$

The notation $[g(x)] \sim \lim_{h \rightarrow 0} g(x) \sim h / g(x) \sim h /$ denotes the jump discontinuity in the function g at x . This shows that at steady-state the pressure difference across each capping end of the tube satisfies an analogue of van 't Hoff's Law with respect to the local concentrations of the solute molecules.

Appendix C. Tables

See Tables C.1 and C.2.

References

- [1] M.Z. Bazant, T.M. Squires, Induced-charge electrokinetic phenomena: Theory and microfluidic applications, *Phys. Rev. Lett.* 92 (6) (2004).

- [2] T. Chou, D. Lohse, Entropy-driven pumping in zeolites and biological channels, *Phys. Rev. Lett.* 82 (17) (1999).
- [3] P. Douzou, Osmotic regulation of gene action, *Proc. Natl. Acad. Sci. USA* 91 (1994) 1657–1661.
- [4] D.D.F. Loo, E.M. Wright, T. Zeuthen, Water pumps, *J. Physiol.* 542.1 (2002) 53–60.
- [5] K.R. Spring, Epithelial fluid transport: A century of investigation, *News Physiol. Sci.* 4 (June) (1999).
- [6] Y.C. Su, L. Lin, A.P. Pisano, A water-powered osmotic microactuator, *J. Microelectromech. Syst.* 11 (6) (2002).
- [7] F. Theeuwes, S.I. Yum, Principles of the design and operation of generic osmotic pumps for the delivery of semisolid or liquid drug formulations, *Ann. Biomed. Eng.* 4 (4) (1976).
- [8] Nardi, Bruinsma, Sackmann, Vesicles as osmotic motors, *Phys. Rev. Lett.* 82 (1999) 5168–5171.
- [9] R. Golestanian, T.B. Liverpool, A. Ajdari, Propulsion of a molecular machine by asymmetric distribution of reaction products, *Phys. Rev. Lett.* 94 (2005) 220801.
- [10] L.E. Reichl, A Modern Course in Statistical Physics, second ed., John Wiley & Sons Inc, New York, 1998.
- [11] R.K. Verma, D.M. Krishna, D. Garg, Formulation aspects in the development of osmotically controlled oral drug deliver systems, *J. Controlled Release* 79 (2002) 7–27.
- [12] F.C. Hoppensteadt, C.S. Peskin, Modeling and Simulation in Medicine and the Life Sciences, Springer-Verlag, New York, 2002.
- [13] J. Keener, J. Sneyd, Mathematical Physiology, Springer-Verlag, 1993.
- [14] R. Lipowsky, From Membranes to Membrane Machines: In Statistical Mechanics of Biocomplexity, Springer-Verlag, Berlin, 1999, pp. 1–32.
- [15] P. Agre, L.S. King, M. Yasui, E.B. Guggino, O.P. Ottersen, Y. Fujiyoshi, A. Engel, S. Nielsen, Aquaporin water channels: From atomic structure to clinical medicine, *J. Physiol.* 542.1 (2002) 3–16.
- [16] P.P. Duquette, P. Bissonnette, J.Y. Lapointe, Local osmotic gradients drive the water flux associated with Na⁺/glucose cotransport, *PNAS* 98 (7) (2001) 3796–3801.
- [17] E.H. Larsen, J.B. Sorensen, J.N. Sorensen, Analysis of the sodium recirculation theory of solute-coupled water transport in small intestine, *J. Physiol.* 542.1 (2002) 33–50.
- [18] L. Reuss, B.H. Hirst, Water transport controversies: An overview, *J. Physiol.* (2002) 1–2.
- [19] P.J. Atzberger, P.R. Kramer, Theoretical framework for microscopic osmotic phenomena, *Phys. Rev. E* 75 (1) (2007).
- [20] P.J. Atzberger, P.R. Kramer, C.S. Peskin, A stochastic immersed boundary method for fluid-structure interactions at microscopic length scales, *J. Comput. Phys.* 224 (2) (2007) doi:10.1016/j.jcp.2006.11.015.
- [21] V.G. Levich, Physico-Chemical Hydrodynamics, Prentice Hall, Englewood Cliffs, NJ, 1962.
- [22] A. Einstein, Investigations on the Theory of the Brownian Movement, Dover Publishing, New York, 1956.
- [23] D. Chandler, Introduction to Modern Statistical Mechanics, Oxford University Press, New York, 1987.
- [24] J.H. van 't Hoff, The role of osmotic pressure in the analogy between solutions and gases, *Z. Phys. Chem.* 1 (1887) 481–508.
- [25] H. Wang, C. Peskin, T. Elston, A robust numerical algorithm for studying biomolecular transport processes, Preprint, 2002.
- [26] C.S. Peskin, The immersed boundary method, *Acta Numer.* 11 (2002) 1–39.
- [27] B. Alberts, A. Johnson, J. Lewis, M. Raff, K. Roberts, P. Walker, Molecular Biology of the Cell, Garland Publishing, 2002.
- [28] L. Evans, Partial Differential Equations, AMS Press, Rhode Island, 2002.
- [29] D.J. Acheson, Elementary Fluid Dynamics, Oxford University Press, Oxford, 1990.
- [30] L.D. Landau, E.M. Lifshitz, Course of theoretical physics, in: Fluid Mechanics, vol. 6, Butterworth-Heinemann, Oxford, 1987.
- [31] W.H. Press, Saul A. Teukolsky, W.T. Vetterling, B.P. Flannery, Numerical Recipes, Cambridge University Press, 2002.
- [32] A.J. Chorin, Numerical solution of the Navier–Stokes equations, *Math. Comp.* 22 (1968) 745.
- [33] M. Holmes, Introduction to Perturbation Methods, Springer, 1995.